Integrating UAV-Based RGB Data and Machine Learning for Accurate Assessment of Soil Salinity

Aphisit Phoolamool[1], *Jurawan* Nontapon[2], *Umesh* Bhurtyal[3], and *Siwa* Kaewplang[1*]

[1] Faculty of Engineering, Mahasarakham University, Kantharawichai District, Maha Sarakham 44150, Thailand
[2] Civil and Construction Management Engineering, Faculty of Science, Chandrakasem Rajabhat University, Bangkok, 10900
[3] Department of Geomatics Engineering, Pashchimanchal Campus, Tribhuvan University, Nepal

Abstract. Soil salinization poses a significant threat to agricultural productivity and sustainability, particularly in semi-arid regions such as Northeast Thailand. This study investigated the potential of unmanned aerial vehicle (UAV)-based RGB photogrammetry combined with machine learning regression models to estimate surface soil salinity at a high spatial resolution. A total of 250 soil samples were collected across the two agricultural seasons and analyzed for electrical conductivity (EC) as a proxy for salinity. RGB imagery was acquired using a DJI Mavic Air 1 UAV and processed to generate orthomosaics at four ground sampling distances (GSDs): 5, 25, 50, and 100 cm. From the imagery, seven color-based indices (GRVI, RGRI, GBRI, RBRI, rn, rg, and rb) were computed and used as input features for three machine-learning models: Generalized Linear Model (GLM), Random Forest (RF), and Support Vector Regression (SVR). The results showed that RF at a GSD of 25 cm achieved the highest prediction accuracy (R^2 = 0.68, RMSE = 4.56). These findings underscore the utility of RGB-derived indices and machine learning models in producing cost-effective, scalable, and accurate salinity maps. This approach is promising for supporting precision agriculture and land management in salt-affected regions.

1 Introduction

Soil salinization is a growing environmental and agronomic challenge that severely constrains agricultural productivity and land sustainability, particularly in arid and semi-arid regions where evaporation surpasses precipitation, and irrigation practices are widespread [1]. Excessive accumulation of soluble salts in the root zone disrupts plant water uptake and alters soil structure, leading to significant reductions in crop yield and progressive land degradation. Traditional field-based methods for assessing soil salinity, such as soil sampling and laboratory electrical conductivity (EC) analysis, although precise, are time-consuming, labor-intensive, and spatially limited, thereby posing constraints for large-scale or real-time monitoring [2].

Unmanned aerial vehicles (UAVs) equipped with remote sensing technologies have emerged as promising tools, enabling high spatial and temporal resolution for precision soil salinity mapping at the field level [3]. UAVs carrying multispectral and hyperspectral sensors have demonstrated strong performance in estimating soil salt content (SSC), particularly when combined with machine learning algorithms [4]. For instance, Zhai [5] showed that combining UAV multispectral reflectance with texture features improved soil salinity prediction accuracy from R^2 = 0.76 to 0.90, with RMSE = 5.13 g/kg. Zhao [6] reported the use of UAV multispectral data to develop SVR, RF, BPNN, and ELM models to estimate the soil salt content. For bare land, the ELM model yielded the highest accuracy (Rv^2 = 0.707, RMSEv = 0.290, RPD = 1.852), whereas for agricultural land with vegetation cover, the BPNN model performed the best (Rv^2 = 0.836, RMSEv = 0.027, RPD = 2.100). Incorporating the red-edge band further improved the estimation accuracy. Similarly, Cui [3] found that RF and Support Vector Regression (SVR) models using vegetation and salt indices yielded strong predictive accuracy for soil salinity at depths of 0–40 cm (R^2 = 0.775), with the best results at shallower depths. To further improve model performance, recent studies have integrated additional data features, such as texture, thermal imagery, LiDAR, and advanced machine learning techniques, including convolutional neural networks (CNN), extreme learning machines (ELM), and backpropagation neural networks (BPNN) [7]. Despite these advances, the high cost and technical complexity of multispectral and hyperspectral UAV sensors have limited their practical adoption, especially in resource-constrained settings.

As a cost-effective alternative, UAVs equipped with RGB cameras, which are commonly used in photogrammetric surveys, are gaining traction. Ivushkin *et al.*[7] used UAV-based RGB imagery to evaluate the effects of soil and water salinity on date palm growth at five arid sites. Seventy-five soil and water samples were analyzed for EC, and imagery was processed to compute the Green Leaf Index (GLI) and segment vegetation cover. GLI correlated strongly with soil EC (R = 0.96) and water EC (R = 0.92), whereas palm-only covered predicted soil EC (R^2 = 0.89) and water EC (R^2 = 0.86), highlighting UAV-RGB as a low-cost, effective salinity monitoring tool. Bermeo et al. [8] utilized RGB drone

* Corresponding author: siwakaewplang@gmail.com

imagery from a DJI Phantom 4 Pro and eight spectral indices to estimate the soil pH, EC, and OM. The results showed a strong correlation between OM and pHindex ($R^2 = 0.55$), while pH and pH_index ($R^2 = -0.39$) and EC and sal_index6 ($R^2 = 0.42$) exhibited moderate correlations. These findings have enabled the development of two models for estimating these variables using RGB imagery. Xu et al. [9] collected 52 soil samples along the coast of Yancheng City, Jiangsu Province, and captured RGB images to assess the relationship between the image brightness, soil salinity, and water content. Soil salinity showed a strong correlation with average brightness, and the Random Forest model achieved high accuracy ($Rv^2 = 0.79$). Integrated with UAV technology, this approach has a strong potential for precision agriculture and land management. These results underscore the potential of RGB-derived metrics as reliable proxies for salinity-related variables in both the soil and plant systems. Moreover, ground sampling distance (GSD) is crucial in UAV-based remote sensing because it defines the spatial resolution of an image. Changes in GSD can significantly impact soil detail capture, data interpretation, model performance, and prediction accuracy [10]. Although UAV-based soil salinity mapping has shown strong potential, few studies have used consumer-grade RGB cameras in arid agricultural settings, particularly with systematic evaluations across multiple ground sampling distances (GSDs) within a single framework. Previous studies have often relied on multispectral or hyperspectral systems or single-resolution RGB imagery. This study integrated UAV-RGB imagery, RGB-derived indices, and machine learning algorithms at multiple GSDs to develop a low-cost approach for salinity monitoring in resource-limited areas.

Building on these developments, this study investigated the integration of UAV-based RGB photogrammetry with machine learning regression models for surface soil salinity estimation. Specifically, the objectives were to (1) evaluate the performance of GLM, RF, and SVR models in predicting soil salinity using RGB reflectance data, and (2) examine the impact of varying ground sampling distances (GSDs) on model accuracy. This study contributes to the development of a low-cost, scalable approach for precision salinity monitoring using UAV-RGB platforms.

2 Research Methodology

2.1 Study Area

This study was conducted over an area of approximately 160,000 square meters in Phon Sim Village, Hua Na Kham Subdistrict, Yang Talat District, Kalasin Province, northeastern Thailand (16°23′53.1″N, 103°16′47.0″E). The area consists of lowland rice fields that are highly susceptible to surface soil salinity, particularly during the dry season when salt crusts commonly appear on the soil surface. This site was selected because it represents the typical environmental conditions of seasonal salinization and is predominantly reliant on rainfed agriculture. The location of the study area is shown in Fig. 1.

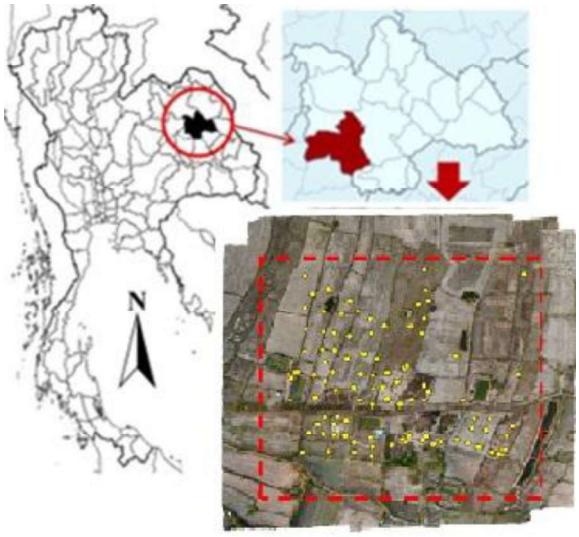

Fig. 1. Location of the study area and soil sampling points.

2.2 Field Sampling of Soil Salinity

Field data were collected during two agricultural seasons: the dry season (February–April 2023) and rainy season (June–August 2023). A total of 250 surface soil samples were obtained from georeferenced locations using a Real-Time Kinematic (RTK) GNSS network with an accuracy greater than 4 cm. All samples were taken from the topsoil layer (0 cm depth) and analyzed in a certified laboratory to determine the electrical conductivity (EC), which was used as a proxy for soil salinity. EC was measured at 25 °C using a 1:5 soil-to-water ratio and a Multi 3420 Set B instrument. Observed EC values ranged from 0.01 to 24.58 dS/m, with a mean of 6.22 dS/m and a standard deviation of 5.05 dS/m. The soil sampling points are shown in Fig. 1, where the UAV imagery (bottom right) illustrates the distribution of these points and the survey boundary (red dashed line).

2.3 UAV Image Acquisition and Georeferencing

A DJI Mavic Air 1 unmanned aerial vehicle (UAV) platform was employed to capture high-resolution aerial imagery under cloud-free weather conditions to minimize atmospheric interference that could affect image quality. The UAV was equipped with an integrated RGB camera capable of capturing images within the visible light spectrum, which is essential for analyzing surface features and vegetation characteristics.

Flight planning was conducted using the PIX4Dcapture application, which enabled the systematic control of flight parameters to ensure adequate spatial coverage and image quality. All flight missions were executed at a constant altitude of 90 m above ground level, providing a suitable ground sampling distance (GSD) for detailed analysis of surface soil characteristics. To reduce geometric distortion and enhance the accuracy of the photogrammetric stitching process, image acquisition was configured with a

forward overlap of 80% and a side overlap of 60%. These overlapping settings allow for the generation of high-quality orthomosaic images and digital surface models (DSM) with continuous spatial coverage and geometric consistency. To improve the geospatial accuracy of the resulting datasets, eight ground control points (GCPs) were strategically distributed across the study area. These GCPs were georeferenced using Real-Time Kinematic Global Navigation Satellite System (RTK GNSS) technology, which provides centimeter-level positional accuracy. The GCPs were incorporated into the photogrammetric processing workflow using the Agisoft Metashape, thereby enhancing the geometric precision and spatial reliability of the final orthomosaic.

2.4 Camera Specifications

In this study, high-resolution aerial imagery was acquired using a DJI Mavic Air 1 unmanned aerial vehicle (UAV), which is equipped with an integrated RGB camera. The camera features a 1/2.3-inch CMOS sensor with a 12-megapixel resolution, capable of capturing true-color images in the visible spectrum. The spectral sensitivity of the sensor spans wavelengths from approximately 450 nm to 660 nanometers (nm), covering the blue (450 nm), green (550 nm), and red (660 nm) regions of the electromagnetic spectrum.

2.5 Image Processing

Image processing and data extraction constituted a crucial phase of this study. High-resolution RGB images acquired by the UAV were processed using Agisoft Metashape Professional to generate accurate spatial datasets suitable for geospatial and salinity analysis.
The photogrammetric workflow consisted of several key steps. First, image alignment is performed to identify the tie points and compute the internal and external parameters of the camera. This was followed by the generation of a dense point cloud representing the three-dimensional spatial distribution of the surface features. Subsequently, surface reconstruction was performed to create a digital surface model (DSM). The DSM was then subjected to orthorectification to correct the distortions caused by camera tilt and terrain variability. This process resulted in the production of an accurate orthomosaic image that preserved the true geographic positions and could be reliably used for further spatial analysis.

To investigate the influence of spatial resolution on salinity detection accuracy and the performance of predictive models, the resulting orthophotos were resampled to four ground sampling distances (GSDs): 5, 25, 50, and 100 cm. This multi-resolution dataset provides a basis for evaluating the effects of spatial resolution on model performance and the robustness of salinity estimation.

2.6 Data Extraction and Index Computation

RGB reflectance values were then extracted from the sample points across the orthomosaic image. To minimize the influence of variable lighting conditions, raw RGB values were normalized using standard reflectance correction equations to ensure consistency and reliability in subsequent analyses.

Normalized reflectance data were used to compute several spectral and vegetation indices, including the Green-Red Vegetation Index (GRVI), Red-Green Ratio Index (RGRI), Green/Blue Ratio Index (GBRI), and pixel-level percentage indices (rn, rg, and rb). The definitions and formulas of these indices are summarized in Table 1. These indices served as input features for the machine learning models designed to estimate and classify soil salinity levels. This integrated processing and extraction workflow enabled the effective interpretation of UAV-acquired imagery with high spatial and spectral resolutions.

Table 1. RGB-Based Spectral and Vegetation Indices.

RGB Index	Formula	Reference
GRVI	(G – R) / (G + B)	[11]
RGRI	R/G	[12]
GBRI	G / B	
RBRI	R / B	
rn	R / (R + G + B)	[13]
rg	G / (R + G + B)	
rb	B / (R + G + B)	

2.7 Model Development

To estimate surface soil salinity from UAV-acquired RGB imagery, this study employed three supervised regression algorithms: a Generalized Linear Model (GLM), Random Forest (RF), and Support Vector Regression (SVR). These models were selected because of their proven effectiveness in environmental modeling and ability to capture both linear and nonlinear relationships within complex datasets [6].

The input features consisted of seven indices derived from UAV-based orthomosaic imagery, including the Green-Red Vegetation Index (GRVI), Red-Green Ratio Index (RGRI), Green-Blue Ratio Index (GBRI), Red-Blue Ratio Index (RBRI), and the normalized red (rn), green (rg), and blue (rb) pixel intensity values. These indices were chosen because of their sensitivity to color and vegetation characteristics, which may reflect patterns of surface soil salinity under natural light conditions.

The dataset comprised 250 samples, of which 70% were used as the training set and 30% as an independent testing set for the final evaluation of the model performance. All input features were standardized using z-score normalization prior to model training. This standardization is particularly important for models such as GLM and SVR, which are sensitive to differences in feature scales. Although Random Forest is inherently scale-invariant and does not require normalization, the same standardized dataset was used for all models to ensure consistency and comparability across different algorithms.

Within the training set, hyperparameter tuning was performed using a grid search approach combined with 5-fold cross-validation, which improved the model generalizability and reduced the risk of overfitting. The GLM was used as a baseline model without any hyperparameter optimization and served as a benchmark for comparison. For the RF model, multiple values of *n_estimators* (50, 75, 100, 150, and 200) were tested, along with *max_depth* and *min_samples_split*. The configuration with *n_estimators* = 100, *max_depth* = 10, and *min_samples_split* = 2 consistently produced the highest average R^2 and lowest average RMSE across the cross-validation folds, while avoiding overfitting. The optimal SVR model was configured with a radial basis function (RBF) kernel using C = 10, epsilon = 0.1, and gamma = 0.01, which is well suited for modeling nonlinear relationships.

All steps, from data preprocessing and model training to validation and evaluation, were performed in RStudio using reliable open-source packages: stats or parsnip for GLM, ranger for RF, and e1071 for SVR with a specified kernel and related parameters.

2.8 Model Evaluation and Statistical Analysis

Model performance was assessed using two standard evaluation metrics: Coefficient of Determination (R^2) and Root Mean Square Error (RMSE). R^2 quantifies the proportion of variance in soil electrical conductivity (EC) explained by the regression models, providing a measure of how well the model captures variability in the observed data. Higher R^2 values indicate a better model fit and greater explanatory power. The RMSE measures the average magnitude of prediction errors, expressed in the same units as the target variable, and is particularly useful for interpreting the model's accuracy in real-world terms. Lower RMSE values indicated that the predictions were closer to the actual observed values.

The combined use of R^2 and RMSE provides a more comprehensive evaluation of model performance: R^2 reflects the proportion of variance explained, whereas RMSE reveals the absolute size of prediction errors. This dual-metric approach allows for a balanced interpretation, as a model may have a high R^2 but still produce large errors, or vice versa. Comparative analyses were performed across different models and ground sampling distances (GSDs) to evaluate predictive accuracy. Equations (1) and (2) were used to compute R^2 and RMSE, respectively, to ensure a consistent and objective model evaluation.

Coefficient of Determination (R^2)

$$R^2 = 1 - \frac{\sum_{i=1}^{n}(y_i - \hat{y}_i)^2}{\sum_{i=1}^{n}(y_i - \bar{y})^2} \quad (1)$$

Root Mean Square Error (RMSE)

$$\text{RMSE} = \sqrt{\frac{1}{n}\sum_{i=1}^{n}(y_i - \hat{y}_i)^2} \quad (2)$$

Where:
y_i = observed value
$\hat{y}_i$ = predicted value
$\bar{y}$ = mean of the observed values
n = number of observations

3 Results

The performance of three regression models, Generalized Linear Model (GLM), Random Forest (RF), and Support Vector Regression (SVR), was evaluated for soil salinity estimation using UAV-derived RGB imagery across four Ground Sampling Distances (GSDs): 5 cm, 25 cm, 50 cm, and 100 cm. Model performance was assessed using the coefficient of determination (R^2) and Root Mean Square Error (RMSE) for both the training (n = 175) and testing (n = 71) datasets. The full performance metrics are listed in Table 2.

Across all models and GSDs, RF consistently outperformed GLM and SVR in terms of the predictive accuracy. The highest RF performance occurred at 25 cm GSD, with R^2 = 0.71 and RMSE = 4.45 (training) and R^2 = 0.68 and RMSE = 4.56 (testing), indicating an optimal balance between capturing spatial heterogeneity in soil salinity, limiting noise, and overfitting. The accuracy declined at coarser resolutions, reaching the lowest at 100 cm GSD (R^2 = 0.50, RMSE = 5.90 in testing). SVR showed intermediate results, peaking at 25 cm GSD (R^2 = 0.61, RMSE = 4.85 for training; R^2 = 0.58, RMSE = 5.24 for testing), but never surpassing RF at any resolution, with a marked drop at 100 cm GSD (R^2 = 0.45, RMSE = 6.71 in testing). GLM consistently performed the worst, with its best results at 25 cm GSD (R^2 = 0.56, RMSE = 5.09 for training; R^2 = 0.56, RMSE = 5.55 for testing) still far below those of RF and SVR. The poorest GLM performance was at 100 cm GSD, where both training and testing R^2 were 0.33 and RMSE reached 7.36 and 7.86, respectively.

The performance comparison of the models using the testing dataset is shown in Fig. 2a and 2b, which present heatmaps of R^2 and RMSE across the models and GSDs. The results indicate that RF achieved the highest accuracy, whereas all models showed a marked decrease in performance at the coarsest resolution (100 cm GSD). The best-performing model (RF at 25 cm GSD) clearly captured the spatial variability of soil salinity, effectively distinguishing between high- and low-salinity zones and demonstrating its capability for fine-scale salinity assessment.

Overall, the results highlight the importance of selecting an appropriate machine learning algorithm and spatial resolution. The RF model, combined with a 25 cm GSD, offers the most effective solution for predicting soil salinity from UAV-based RGB imagery.

Table 2. Performance metrics (R^2 and RMSE) of GLM, RF, and SVR models for soil salinity prediction across different GSD levels.

Model	GSD (cm)	Training		Testing	
		R^2	RMSE	R^2	RMSE
GLM	5	0.42	6.35	0.40	6.84
	25	0.56	5.09	0.56	5.55
	50	0.48	5.68	0.46	5.70
	100	0.33	7.36	0.33	7.86
RF	5	0.62	4.91	0.59	5.38
	25	0.71	4.45	0.68	4.56
	50	0.64	4.75	0.61	5.09
	100	0.51	5.65	0.50	5.90
SVR	5	0.48	5.60	0.46	5.95
	25	0.61	4.85	0.58	5.24
	50	0.57	5.20	0.56	5.50
	100	0.45	6.13	0.45	6.71

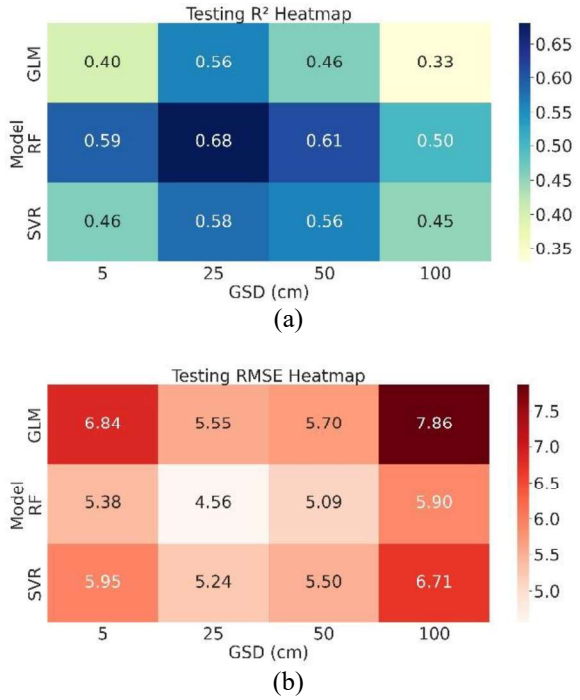

Fig 2. Heatmap comparison of (a) R^2 and (b) RMSE for soil salinity prediction using machine learning models across different GSDs.

4 Discussion

The integration of UAV-based RGB photogrammetry and machine learning (ML) models in this study demonstrated promising potential for mapping surface soil salinity in a semi-arid agricultural landscape. The Random Forest (RF) model achieved the highest predictive accuracy, particularly at the 25 cm ground sampling distance (GSD), with an R^2 of 0.68, and RMSE of 4.56 on the testing dataset. Although these results reflect acceptable model performance, they are somewhat lower than those reported in previous studies using multispectral or hyperspectral data, which often exceeded the R^2 values of 0.80 [5].

One plausible explanation for the moderate R^2 in this study lies in the spectral limitations of the RGB sensors. Unlike multispectral systems that capture reflectance in narrow, salt-sensitive wavelengths (e.g., near-infrared and shortwave infrared), RGB sensors operate within the visible spectrum (450–660 nm), which may not directly capture soil salinity signatures. However, recent studies [8, 9] have shown that RGB-derived indices can indirectly reflect salinity stress through vegetation responses or surface texture variations, especially when analyzed using nonlinear ML algorithms such as RF or ANN.

The choice of a 25 cm GSD proved optimal, corroborating the findings of Yao et al. [10], who emphasized that medium spatial resolutions strike a balance between capturing sufficient spatial detail and avoiding noise introduced by very fine resolutions (e.g., 5 cm). At coarser resolutions (50–100 cm), critical spatial patterns, such as salt crusts or micro-topographic variations, may be lost due to pixel aggregation, explaining the performance degradation observed across all models at 100 cm GSD.

Although RF outperformed the Generalized Linear Model (GLM) and Support Vector Regression (SVR) in all scenarios, its R^2 remained below 0.70. This suggests that the input features, although relevant, may not fully capture the spatial variability of soil salinity. One potential improvement could involve incorporating additional texture-based features extracted from high-resolution RGB images, as highlighted by [5], who reported R^2 improvements from 0.76 to 0.90 when combining reflectance and texture attributes. Furthermore, the integration of ancillary data such as soil moisture, elevation, or terrain derivatives may enhance model robustness.

The lower performance of the GLM model, particularly at 100 cm GSD (R^2 = 0.33), reflects its limited capacity to capture the nonlinear interactions between spectral indices and soil salinity. This aligns with earlier findings by Hu [4], which emphasize the necessity of nonlinear models when dealing with complex soil-environment relationships.

Finally, while SVR showed moderate performance, its sensitivity to parameter tuning and feature scaling may have limited its generalizability. Future work could explore more advanced models such as convolutional neural networks (CNNs) or ensemble learning frameworks (e.g., stacking RF and SVR), which have shown superior performance in similar environmental applications [3, 6].

The predicted salinity map (Fig. 3) aligned well with the landscape, with high salinity in low-lying, poorly drained zones and low salinity in higher, well-drained terrains. This confirms the effectiveness of UAV-RGB imagery with the Random Forest model in linking salinity to topography and supporting targeted management. Overall, the UAV-RGB with machine learning offers a cost-effective tool for soil salinity assessment, although moderate R^2 values suggest the need for richer input features, hybrid models, and additional environmental data.

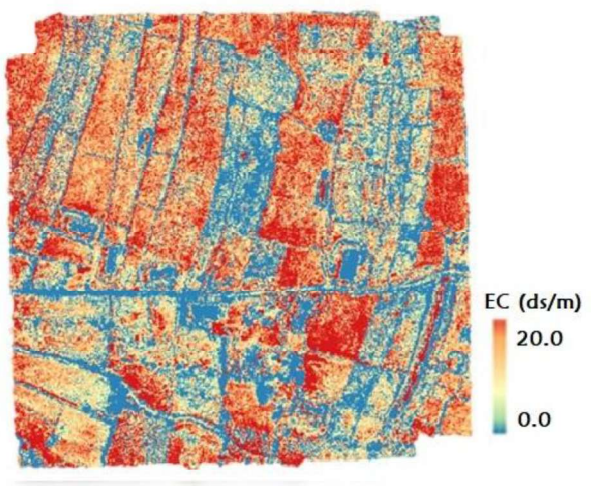

Fig. 3. Predicted Surface Soil Salinity Map Derived from UAV-RGB Imagery and Random Forest Model at 25 cm GSD.

5 Conclusion

This study demonstrated the effectiveness of integrating UAV-based RGB photogrammetry with machine learning models for surface soil salinity estimation in salt-affected agricultural areas. Using accessible RGB imagery and color-based indices, soil electrical conductivity (EC) was successfully predicted with high accuracy. The Random Forest (RF) model, particularly at a ground sampling distance (GSD) of 25 cm, achieved the best performance (R^2 = 0.68; RMSE = 4.56), indicating that moderate spatial resolution strikes an optimal balance between detail and model generalizability.

These findings highlight the potential of the RGB-derived indices as reliable input features for salinity mapping. This approach offers a low-cost and scalable alternative to multispectral and hyperspectral systems, making it particularly valuable in resource-constrained contexts. RGB sensors mounted on commercially available UAVs enable rapid data acquisition and processing, thereby supporting timely decisions for land management and agricultural planning.

Overall, the results reinforce the utility of combining RGB photogrammetry with machine learning as a practical solution for fine-scale soil-salinity monitoring. Future research should explore the integration of additional features, such as surface texture and temporal dynamics, and test the model across various agro-ecological zones to enhance its robustness and applicability.

Funding: This research project was financially supported by the Faculty of Engineering at Mahasarakham University.

References

1. Devkota, K. P., Devkota, M., Rezaei, M., Oosterbaan, R., Managing salinity for sustainable agricultural production in salt-affected soils of irrigated drylands. Agricultural Systems. **198**, 103390 (2022).
2. Metternicht, G. I., Zinck, J. A., Remote sensing of soil salinity: potentials and constraints. Remote sensing of environment. **85**(**1**), 1–20 (2003).
3. Cui, J., Chen, X., Han, W., Cui, X., Ma, W., Li, G., Estimation of soil salt content at different depths using uav multi-spectral remote sensing combined with machine learning algorithms. Remote Sensing. **15**(**21**), 5254 (2023).
4. Hu, J., Peng, J., Zhou, Y., Xu, D., Zhao, R., Jiang, Q., Fu, T., Wang, F., Shi, Z., Quantitative estimation of soil salinity using uav-borne hyperspectral and satellite multispectral images. Remote Sensing. **11**(**7**), 736 (2019).
5. Zhai, J., Wang, N., Hu, B., Han, J., Feng, C., Peng, J., Luo, D., Shi, Z., Estimation of soil salinity by combining spectral and texture information from uav multispectral images in the tarim river basin, china. Remote Sensing. **16**(**19**), 3671 (2024).
6. Zhao, W., Zhou, C., Zhou, C., Ma, H., Wang, Z., Soil salinity inversion model of oasis in arid area based on uav multispectral remote sensing. Remote Sensing. **14**(**8**), 1804 (2022).
7. Ivushkin, K., Bartholomeus, H., Bregt, A. K., Pulatov, A., Franceschini, M. H., Kramer, H., van Loo, E. N., Roman, V. J., Finkers, R., UAV based soil salinity assessment of cropland. Geoderma. **338**, 502–512 (2019).
8. Álava Bermeo, M., García Solórzano, A., Pacheco Gil, H., Model for estimating soil chemical properties with rgb drone images. Enfoque UTE. **15**(**4**), 19–26 (2024).
9. Xu, L., Ma, H., Wang, Z., Soil salinity and soil water content estimation using digital images in coastal field: a case study in yancheng city of jiangsu province, china. Chin. Geogr. Sci. **32**(**4**), 676–685 (2022). https://doi.org/10.1007/s11769-022-1293-1.
10. Yao, H., Qin, R., Chen, X., Unmanned aerial vehicle for remote sensing applications—a review. Remote sensing. **11**(**12**), 1443 (2019).
11. Ballester, C., Brinkhoff, J., Quayle, W. C., Hornbuckle, J., Monitoring the effects of water stress in cotton using the green red vegetation index and red edge ratio. Remote Sensing. **11**(**7**), 873 (2019).
12. Wan, L., Li, Y., Cen, H., Zhu, J., Yin, W., Wu, W., Zhu, H., Sun, D., Zhou, W., He, Y., Combining uav-based vegetation indices and image classification to estimate flower number in oilseed rape. Remote Sensing. **10**(**9**), 1484 (2018).
13. Li, S., Yuan, F., Ata-UI-Karim, S. T., Zheng, H., Cheng, T., Liu, X., Tian, Y., Zhu, Y., Cao, W., Cao, Q., Combining color indices and textures of uav-based digital imagery for rice lai estimation. Remote Sensing. **11**(**15**), 1763 (2019).